

Power quality enhancement by SiC Active Power Filters in Oil and Gas Platforms

Laís A. Vitoi
 Graduate Program in Electrical
 Engineering
 Federal University of Minas Gerais
 (UFMG)
 Belo Horizonte, Brazil
 laisvitoi@gmail.com

Danilo I. Brandao
 Graduate Program in Electrical
 Engineering
 Federal University of Minas Gerais
 (UFMG)
 Belo Horizonte, Brazil
 dibrandao@ufmg.br

Elisabetta Tedeschi
 Department of Electric Power
 Engineering
 Norwegian University of Science and
 Technology (NTNU)
 Trondheim, Norway
 Elisabetta.tedeschi@ntnu.no

Abstract—This paper presents a study for active power filters’ (APFs) application in a typical offshore O&G platform, where reactive power compensation and current harmonic mitigation are often needed to meet minimum power quality requirements. As size and weight are critical constraints in offshore installations, possible benefits of using Silicon Carbide (SiC) switches for the APF implementation are also investigated. Different compensation strategies have been compared, varying the connection point of the APF between two different voltage levels and assigning the APFs different compensation targets. Improvements in Power Quality (PQ) indexes as well as APFs rating, efficiency and design complexity have been considered for both SiC and Silicon-based solutions to identify trade-offs suitable for the considered application.

Keywords— Active power filter, O&G platform, Power Quality, Wide band-gap semiconductors

I. INTRODUCTION

Despite the growth of renewable energy, gas and oil are forecasted to remain the two main energy resources until 2050 and beyond. The offshore exploration and drilling of oil and gas (O&G) has gained momentum over the last decades [1], [2], and about 27% and 30% of the gas and oil extractions, respectively, are currently performed offshore. However, the power supply to O&G platforms still represents an industrial challenge. In particular, the distance between the platform and the main land, and the high local power requirements (5-200 MW) are critical factors, often preventing the cable-connection to shore for technical and/or economic reasons. In all those cases, power generation is provided by onboard gas turbines or diesel generators and the local electric grid is operated as an isolated network, characterized as a weak grid.

Fig. 1 illustrates the typical electric grid in an O&G platform, whose main components are: synchronous generators coupled to the gas turbines, power transformers, power converters and loads. Although DC-based power distribution for O&G drilling applications has recently been under investigation [3], AC systems represent the state of the art. However, the presence of large power loads (e.g., pumps, compressors, etc.), the increasing use of electric drives, coupled to generator impedances (12-25%) that are significantly higher than those of grid connected power systems contribute to the deterioration of the local power quality. A major drawback of these AC power systems is the inherent presence of reactive power (with power factors, PF, that in extreme cases can be as low as 0.36 [4]), resulting in higher currents and increased power losses in the distribution lines. Additionally the connection of power converters, typically for AC and DC drives, results in non-linear loads, and hence harmonic pollutions, with reported THDv and THDi as high as 12% and 27%, respectively [4].

The tight space and weight constraints of offshore O&G applications make the deployment of any additional devices occupying deck-space critical, as proved by the recent trend to place more processing equipment subsea [3]. On the other hand, a single power-quality incident offshore can cost up to 750.000 EUR per day [4]. Several methods have been proposed to compensate the reactive power and harmonic components generated by industrial loads, and a few contributions also targeted O&G drilling rigs, considering both passive and active solutions [5]–[7]. In particular, Shunt Active Power Filters (SAPFs) based on three-phase Voltage Source Converters (VSCs) are well-suited for this application,

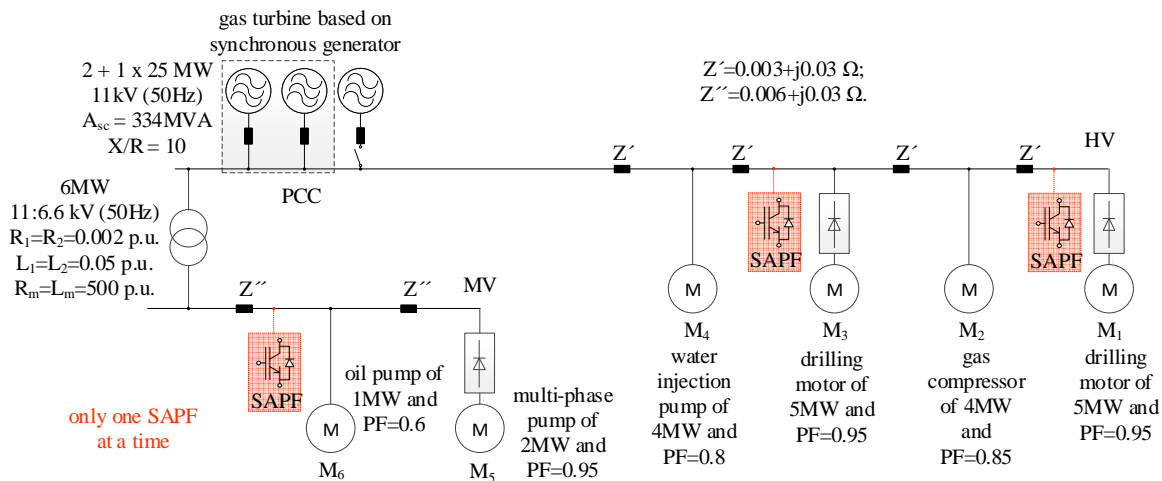


Fig. 1. Schematic diagram of the isolated grid of an offshore O&G platform.

as they exploit the converter capability of producing reactive power without bulky energy storage components and they are flexible in the compensation of multiple harmonics, up to high orders, in addition to reactive power. Hence, they are smaller, lighter, faster, and with better performances at reduced voltages compared to other solutions. However, an analysis benchmarking PQ performance and APF designs for the specific application is missing in the previous literature.

For this reason, the paper focuses on the design of a SAPF to be used in an offshore O&G platform, considering the impact of different SAPF locations and investigating how specific design considerations, including the use of wide-bandgap semiconductors and proper output filter design in the converter, can contribute towards size and loss reduction and high compensation performance. It also comments on two compensation strategies, i.e., resistive load synthesis and sinusoidal current synthesis, and their respective suitability for the considered application.

The structure of the paper is as follows: in Section II the main industrial processes that take place on an O&G platform and the required electrical power components are discussed; Section III presents the theoretical and mathematical analysis of the SAPF; in Section IV, the selected case study and the results are presented. Finally, Section V includes discussion and conclusions.

II. PROCESSING OF OIL AND GAS ON OFFSHORE PLATFORMS AND RELATED POWER SUPPLY

On a platform, the process of transforming the fluid extracted from the well into marketable products, including cleaning of waste products such as produced water, requires several stages and large equipment with high power demand. Each oil and gas platform has typically several wells, divided into production and injection wells. While the former are used for production of oil and gas the latter are drilled to inject gas or water into the reservoir to support its pressure and push the fluid towards the production well (enhanced oil recovery). Such process requires large compressors or pumps, having a power consumption from a few MW up to more than 25 MW [8]. In modern installations, electrical submerged pumps, up to a few MW, are also inserted into the well.

Moreover, as the well-stream may consist of crude oil, gas, condensates, water and various contaminants, a separator is needed to divide the different components. As the gas coming from separators may have low pressure, it must be recompressed to be transported. Several types of compressors can be used for such task, with the largest centrifugal compressors having a power in the 80 MW range [2]. Metering, storage and export process conclude the production cycle, while treatment of chemicals and waste water is also needed.

Power generation on O&G platforms typically relies on local gas turbines (GTs) driving synchronous generators (SGs), as shown in Fig.1. Their capacity range is usually between few MW and 40 MW per turbine [9]. The number of turbines on the platforms is often limited to three or four, with one used as a back-up for reliability purposes. SGs and GTs are connected to the highest voltage bus on the platform.

Two main AC voltage levels, e.g. 6.6 kV and 11 kV, hereafter defined as medium voltage (MV) and high voltage (HV), respectively, are normally used for the platform distribution system. Large compressors, pumps and drilling

rigs are the main loads being driven by electric motors. They typically constitute 75-80% of the total electric load on the platform and, as their individual power consumption is in the multi-MW range (up to several dozens of MW), they are typically connected to the HV bus. A low voltage bus (LV, e.g. 400 V) is also present to allow the interconnection of several smaller loads (e.g. lightning, living-quarter loads, possibly also DC).

Due to the variety of voltage levels and load types and characteristics, the use of both transformers and power electronic converters is required. Power converters, particularly large 6- or 12- pulse rectifiers [10] coupled to fully-controlled inverters, are increasingly connected to electric motors for drilling, pumping, etc., in order to allow variable speed operation for efficiency increase. This however, leads to harmonic generation and power quality deterioration [10].

This paper analyzes the O&G platform electric system shown in Fig. 1 and further described in Section IV. It has different loads types connected to both HV and MV buses. Table I summarizes the loads parameters.

TABLE I. DESCRIPTION OF THE LOADS PARAMETERS.

Load	Type	Active power-P	PF	Apparent power-A	$\sqrt{A^2 - P^2}$
M1	Drilling motor	5 MW	0.95	5.36 MVA	1.93 MVA
M2	Gas compressor	4 MW	0.85	4.71 MVA	2.48 MVA
M3	Drilling motor	5 MW	0.95	5.35 MVA	1.90 MVA
M4	Water injection pump	4 MW	0.8	5.00 MVA	3.00 MVA
M5	Multi-phase pump	2 MW	0.95	2.10 MVA	0.64 MVA
M6	Oil pump	1 MW	0.6	1.67 MVA	1.33 MVA

III. THEORETICAL AND MATHEMATICAL ANALYSIS OF SHUNT ACTIVE POWER FILTER

In this paper, the SAPF has been adopted as compensation system for reactive power and harmonic pollution in an offshore O&G platform. A three-phase 2-level VSC is selected as APFs topology. It consists of three arms, each comprising one half bridge. Therefore, six power switches are required. Each of the switches can be realized with multiple power semiconductor devices connected either in series or in parallel, depending on the voltage and current rating. In addition to the switching stage, the SAPF requires some passive components, such as a DC side capacitor and an output filter to be connected to the AC grid. Fig. 2 illustrates a simplified structure of a SAPF. The following subsections detail each part of the SAPF.

A. Power semiconductor devices

Traditionally the power devices are made up of silicon (Si) material, but with the increasing demand on efficiency, high voltages and high switching frequencies, the Si switches may not be able to satisfy all the requirements. The emerging of silicon carbide (SiC) devices brings new design possibilities for the medium-voltage high-power converters. The SiC technology presents superior material properties when compared to the Si counterpart. The higher wide band-gap,

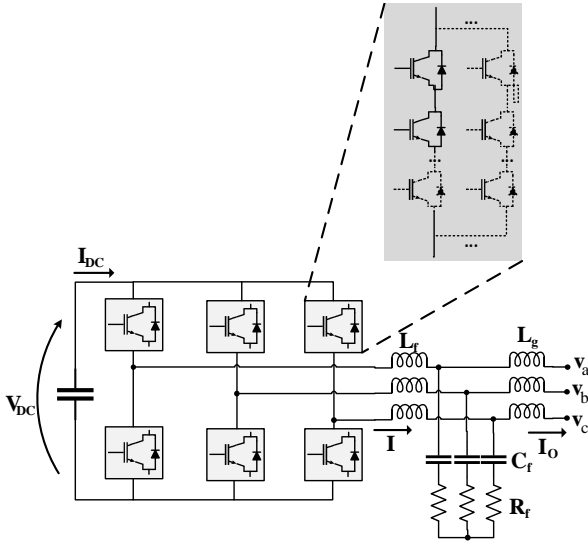


Fig. 2. Structure of the SAPF.

dielectric breakdown field strength and thermal conductivity allow to increase the operational switching frequency and voltage without increasing the losses. With a higher switching frequency, the passive filtering components have smaller size and the cooling requirements can be relaxed, therefore, the overall system volume and weight are reduced [11-15]. In order to compare the performance, both technologies, i.e. Si and SiC, are analyzed in the paper.

An association of series and parallel switches is necessary to comply with the requirements of the circuit voltage and current [16]. The number of devices in series (n_{series}) and in parallel ($n_{parallel}$) for a two-level converter can be calculated by (1) and (2) respectively. I_{device} is the direct current, V_{device} is the blocking voltage of the switch and SF is a voltage safety factor taking into account the typical values commonly used and reported in the datasheet.

$$n_{parallel} = \frac{I_{DC}}{I_{device}} \quad (1)$$

$$n_{series} = \frac{V_{DC}}{V_{device} \cdot SF} \quad (2)$$

The losses calculation follows the methodology proposed by [14], [17] and [18] and includes both conduction and switching losses. The average conduction losses (P_{cond}) of each device are given in (3), where V_0 is the threshold voltage, R_0 the slope resistance, I_{av} and I_{rms} are the average and root mean square currents respectively.

$$P_{cond} = V_0 \cdot I_{av} + R_0 \cdot I_{rms}^2 \quad (3)$$

The switching losses for a two-level converter can be calculated as given in (4), where n_{device} is the number of devices used, f_{sw} is the switching frequency, E_{on} and E_{off} are the switching loss energy obtained from the datasheet and testing materials. Since the datasheet switching loss energy are measured for a specific V_{ref} , it is necessary to correct the losses for the actual voltage across each device (V_{CC}).

$$P_{sw,2L} = n_{device} \cdot f_{sw} \cdot (E_{on} + E_{off}) \cdot \frac{V_{CC}}{V_{ref}} \quad (4)$$

B. Passive components

The proper design of the output filter is of great importance for performance and size [11], [12] of the SAPF. Different strategies for the design of the passive components are reported in literature. For this study the LCL configuration, illustrated in Fig. 2, has been considered the most suitable. The LCL arrangement is capable to filter higher order harmonics with lower cost, and reduced overall weight and size compared with the L filter [19]. The filter design follows the methodology presented in [19]; C_f , L_f , L_g , and R_f can be calculated by (5), (6), (7) and (8) respectively.

$$C_f = 0.05 \cdot C_b \quad (5)$$

$$L_f = \frac{V_{DC}}{6 \cdot f_{sw} \Delta I_{Lmax}} \quad (6)$$

$$L_g = \frac{\sqrt{\frac{1}{k_a^2} + 1}}{C_f w_{sw}^2} \quad (7)$$

$$R_f = \frac{1}{3w_{res} C_f} \quad (8)$$

where ΔI_{Lmax} is the maximum current ripple at the inverter output, k_a is the desired harmonic attenuation, C_b is base capacitance and w_{res} is the resonant frequency.

C. Control scheme

The SAPF's control block diagram is shown in Fig. 3. The control scheme has a faster inner loop to regulate the current, and a slower outer loop to control the DC voltage. V_{DC}^* is the DC voltage reference, i^* is the AC current reference, s^* is the synthesis signal that can be the normalized Point of Common Coupling (PCC) voltage, or can come from a PLL (Phase Locked Loop), depending on the selected compensation strategy [21]. C_v and C_i are the controllers of the voltage and current loops, respectively.

Two compensation strategies could be implemented: resistive load synthesis (RLS) and sinusoidal current synthesis (SCS) [22]. The reference generator block is responsible for synthesizing the two types of compensation and create the reference current signal (i^*).

The sinusoidal current synthesis results in a sinusoidal line current, regardless of the voltage waveform at the PCC. The resistive load synthesis emulates a resistive load behaviour; therefore, the line current has the same waveform as the PCC voltage, changing only its amplitude. The resistive load synthesis minimizes the current rms value for a given active power demand and has a damping effect for possible resonances in the circuit [22].

The reference current signal i^* can be calculated as given by (9) for the RLS, and by (10) for SCS.

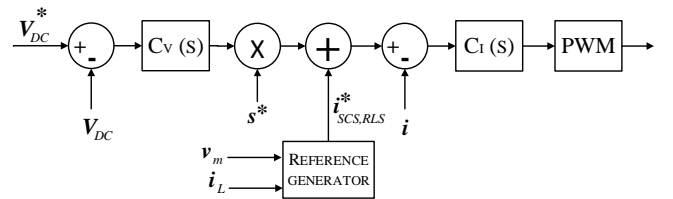


Fig. 3. Control block diagram.

$$i_{RLS}^* = i_{Lm} - \frac{P}{\sqrt{2}} v_m \quad (9)$$

$$i_{SCS}^* = i_{Lm} - \frac{P}{\sqrt{2}} v_m^1 \quad (10)$$

where i_{Lm} and v_m are the measured line current and voltage in each phase ($m = a, b, c$) respectively, P is the total active power, V is the collective value of the voltage at the PCC and the superscript 1 represents the fundamental value of the variable.

IV. SIMULATION RESULTS AND ANALYZES

The isolated grid of Fig. 1 has been used as test-case and simulated in Matlab/Simulink. It includes the GTs' SGs (2x25 MVA). Two large 5 MW drilling motors controlled by a Variable Speed Drive (VSD) with a 6-pulse rectifier and a 4 MW water pump-Induction Motor (IM) and a 4 MW compressor directly connected to the grid are integrated into the HV bus. Another directly-connected IM motor (1 MW) is integrated into the MV bus, together with a 2 MW drive-controlled multi-phase pump. The main test-case parameters are shown in Fig. 1, Table I and Table II. Although only one SAPF is to be connected to the grid, several different options are considered for its connection point and compensation objectives, corresponding to different local compensation strategies. The details are presented in Table II. The effect of such choices on the final PQ indexes at the HV bus (PCC) is assessed. Moreover, for each case, two variants are considered, where (a) refers to the SAPFs implementation using Si-based IGBTs, for which two different voltage ratings have been considered (i.e., 3.3kV Si-IGBT 5SNA 1200E33100 [17] and 6.5kV Si-IGBT 5SNA 0400J650100 [20]) and (b) refers to the SAPFs using SiC-based MOSFETs (10kV SiC MOSFET/SiC-JBS diode [23]). The 3.3 kV and 6.5 kV Si IGBTs have a maximum blocking voltage of 3.3 kV and 6.5 kV and a current capacity of 1200 A and 400 A respectively and the SiC Mosfet has a blocking voltage of 10 kV and 100 A capacity.

As mentioned earlier, two compensation strategies are theoretically possible: resistive load synthesis (RLS) and sinusoidal current synthesis (SCS). As the O&G platform is characterized as a weak system, the SCS compensation by commanding a sinusoidal current independently of the voltage waveform may force additional non-linearities in the system, which in turn can trigger voltage resonances. In view of this fact, only the RLS results are shown and analyzed hereafter.

As shown in Table III, when no SAPF is connected, the power factor measured at the HV bus (as ratio between active power and apparent power) is 0.91 and THDi = 13.6%. The SAPF is activated at $t = 0.1$ s, and controlled in RLS mode in order to obtain a purely active current (i.e. unity power factor and current proportional to the local voltage waveform) at the selected bus. PQ performance indexes are similar independently on the type semiconductors used and they are compared in Table III. Case 1 utilizes the SAPF with the smallest power rating, connected to the MV. Although succeeding in the local compensation task (it has PF at MV = 1, with equal current and voltage THDs of 5.5 %), the improvement of corresponding indexes at PCC is limited, as the power rating of the MV loads is significantly smaller than that of the HV ones. When the SAPF is connected to the HV bus in order to compensate only the harmonic distortion of one local load, M1, (Case 2), the required rating is only slightly

increased compared to Case 1, but the THDv at PCC is reduced below 5%.

The PF at PCC remains almost unchanged due to the presence of large uncompensated linear and non-linear loads at HV in both cases. Finally, in Case 3 the APF properly compensates all the HV loads except M4 and THDv and THDi at PCC are reduced to 1.37% and 1.91%, respectively with PF=0.98. However, the goal is achieved at the expense of a significantly higher SAPF rating. As an example, Figs. 4 and 5 illustrate the active power, the reactive power, the PCC current and voltage, and the SAPF current obtained in Case 3.

Following the methodology presented in Section III, the switching losses associated to the inverter, the total number of switching components and the required values of the passive LCL filter considering both technologies: Si and SiC, were calculated. Two Si-IGBTs are analyzed and the comparison is

TABLE II. DESCRIPTION OF THE CASES STUDIES.

Case	Compensated loads	Comp. objective	APF bus	DC volt.	Semic. used
1.a	M6 and M5	SAPF at MV bus	MV (6.6 kV)	12 kV	Si
1.b	M6 and M5	SAPF at MV bus	MV (6.6 kV)	12 kV	SiC
2.a	M1	SAPF at M1	HV (11 kV)	18 kV	Si
2.b	M1	SAPF at M1	HV (11 kV)	18 kV	SiC
3.a	M1, M2 and M3	SAPF at a set of loads	HV (11 kV)	18 kV	Si
3.b	M1, M2 and M3	SAPF at a set of loads	HV (11 kV)	18 kV	SiC

TABLE III. POWER QUALITY PERFORMANCE ANALYSIS.

	Base Case: No comp	Case 1	Case 2	Case 3
APF bus voltage (kV)	-	6.6	11	11
APF current (A)	-	146.2	95.75	240.5
APF rating (MVA)	-	1.67	1.82	4.57
THD v - @PCC (%)	5.78	5.5	4.6	1.37
THD i - @PCC (%)	13.6	12.43	7.9	1.91
PF - @PCC	0.91	0.94	0.93	0.98

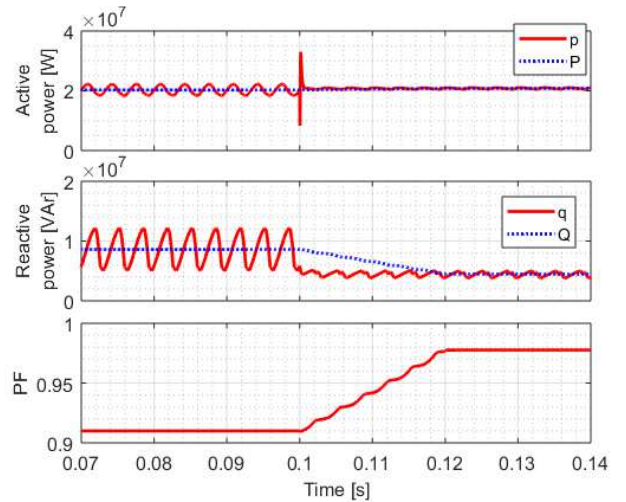


Fig. 4. Active (top) and reactive (middle) power and PF (bottom) at the HV bus (PCC) in Case 3.

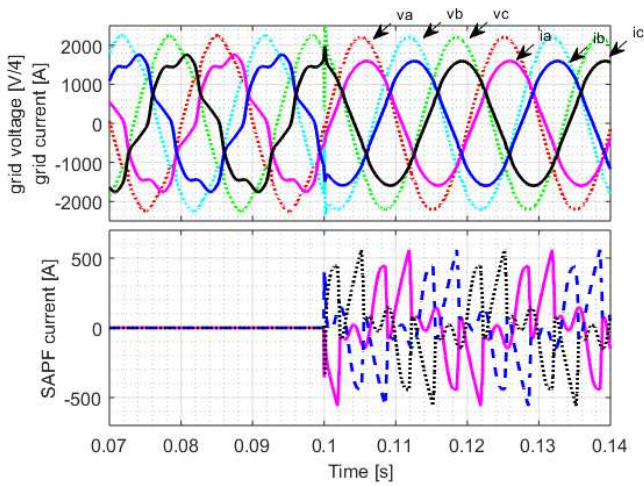


Fig. 5. PCC voltage and current (top), SAPF current (bottom) in Case 3.

shown in Table IV. As can be observed, using the 6.5 kV IGBT the number of components required is lower, but the total loss is higher than for the 3.3 kV IGBT. For this reason the 3.3 kV solution (a-cases) is selected to be further compared to the SiC option (b-cases) in the various cases. Table V shows the results for the 3,3kV Si-IGBT and 10 kV SiC-Mosfet. It is considered only the IGBTs/Mosfets losses and they are calculated from the data in the datasheet [17] and reference paper [23]. The results indicate that the use of SiC significantly reduces switching and conduction losses and is better suited for lower current applications, where it provides lower switches' count than Si-counterparts. In terms of LCL filter sizing the most compact ones are those based on SiC that provide smaller volume and lighter weight, as expected.

V. DISCUSSION AND CONCLUSIONS

The final selection of an APF to be applied in an O&G platform is a complex decision that emerges as a trade-off among several factors, such as the APF rating, design (e.g., output filter design, number and type of semiconductor switches, etc.), operation (e.g., losses) and overall PQ performance it can provide (i.e., THD_v, THD_i, PF, etc.). The different aspects considered in this study can be visually summarized in Fig. 6, which is proposed as a preliminary selection tool to orient the choice of the SAPF. All the parameters shown on the different axes for the various cases are normalized over their maximum value. Assuming that they are equally weighted, the smaller the area delimited by the line corresponding to one case, the better that SAPF alternative is considered. It can be seen, for example, that Case 2.b (SiC based SAPF connected to HV and only compensating the local load M1) offers the best trade-off, with intermediated PQ performance, but low total losses, semiconductor count and APF rating. As a comparison, the corresponding Si-solution (Case 2.a), despite providing equivalent PQ performance is penalized in terms of APF design (more switches and bigger filter) and higher losses, and should be disregarded.

Overall, this paper has shown that SAPF can be a good solution for isolated power grids, such as O&G platforms, where deteriorated power quality requires reactive and harmonic compensation, but tight space and weight constraints are present. In particular, the advantage of a SiC-based implementation of such SAPF have been presented and quantified.

TABLE IV. COMPARISON OF THE SI-IGBT.

	Case 1	Case 2	Case 3	Case 1	Case 2	Case 3
Semiconductor	Si					
Switching frequency	2 kHz					
Voltage safety factor (SF)	0.6					
Model	5SNA 1200E330100 – 3.3kV			5SNA 0400J650100 – 6.5 kV		
RMS current of SAPF (A)	146.2	95.75	240.5	146.2	95.75	240.5
Number of devices	36	54	54	24	30	30
Switching losses (kW)	58.72	74.53	113.9	88.27	79.63	173.3
Conduction losses (kW)	1.28	0.83	5.21	3.12	1.83	11.57
Total losses (kW)	60	75.4	119.1	91.4	81.5	184.9

TABLE V. RESULTS OF THE SAPF DESIGN.

Parameter	Case 1a	Case 1b	Case 2a	Case 2b	Case 3a	Case 3b	
Connection point	MV	MV	HV	HV	HV	HV	
Semiconductor device used	Si	SiC	Si	SiC	Si	SiC	
Switching frequency (kHz)	2	10	2	10	2	10	
RMS current of SAPF (A)	146	146	96	96	240	240	
Switching losses (kW)	58.7	42.7	74.5	32.0	114	96.1	
Conduction losses (kW)	1.3	5.1	0.8	6.6	5.2	13.9	
Total losses (kW)	60	47.8	75.3	38.6	119.2	110	
Number of devices	36	24	54	18	54	54	
$\Delta I_{L,max}$	25 % of $I_{SAPF-peak}$ value						
k_a	0.2						
Passive Filter requirements	L_f (mH)	19.3	3.9	44.3	8.9	17.6	3.5
	L_g (mH)	5.3	0.2	14.9	0.6	4.6	0.2
	C_f (μ F)	7.2	7.2	2.5	2.5	8.3	8.3
	r_f (Ω)	7.9	1.8	22.1	4.9	6.9	1.5
Resonance frequency (kHz)	0.92	4.19	0.94	4.22	0.92	4.19	

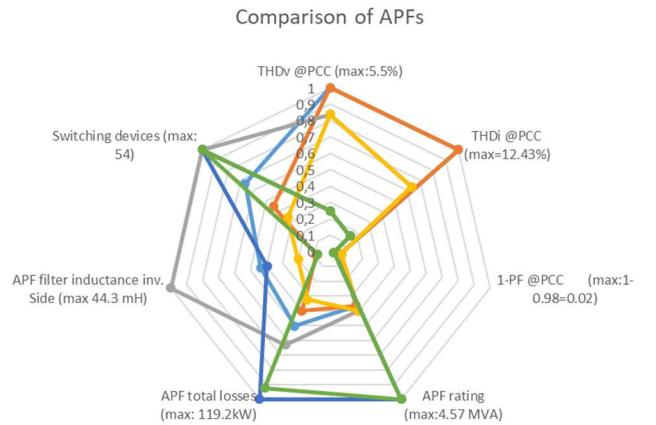


Fig. 6. Comparison of APFs solutions. (light blue: case 1.a; orange: case 1.b; grey: case 2.a; yellow: case 2.b; dark blue: case3.a; green: case3.b).

ACKNOWLEDGMENT

The authors acknowledge the financial support received by the Research Council of Norway under the grant number 261735, project "Norwegian-Brazilian collaboration on Power Theories and Cooperative Control for Renewable Energy Integration (NB_POCCREI)".

REFERENCES

- [1] R. A. Durham and T. R. Brinner, "Oilfield electric power distribution," in 2014 IEEE Petroleum and Chemical Industry Technical Conference (PCIC), 2014, pp. 429–442.
- [2] K. Rajashekara, "Electrification of Subsea Systems Requirements and Challenges in Power Distribution and Conversion," CPSS Trans. Power Electron. Appl., vol. 2, no. 4, pp. 259–266, Dec. 2017.
- [3] B. M. Grainger, G. F. Reed, T. E. McDermott, Z. Mao, V. Kounev and D. Tipper, "Analysis of an offshore medium voltage DC microgrid environment " 2014 IEEE PES T&D Conference & Exposition, Chicago, 2014.
- [4] K. Schipman and F. Delincé, "The importance of good power quality," ABB Power Qual. Prod., p. 1–20, 2010.
- [5] M. Kale and E. Özdemir, "Harmonic and reactive power compensation with shunt active power filter under non-ideal mains voltage," Electr. Power Syst. Res., vol. 74, no. 3, pp. 363–370, 2005.
- [6] V. K. A. Shankar and N. S. Kumar, "Implementation of Shunt Active Filter for Harmonic Compensation in a 3 Phase 3 Wire Distribution Network," Energy Procedia, vol. 117, pp. 172–179, 2017.
- [7] A. R. Dekka, A. R. Beig, and M. Poshtan, "Comparison of passive and active power filters in oil drilling rigs," in 11th International Conference on Electrical Power Quality and Utilisation, 2011, pp. 1–6.
- [8] T. Waterfield, B. Germain "The world largest injection pumps", Sulzer Technical Review Vol. 4, 2003
- [9] H. Devold, "Oil and Gas production Handbook" ABB ATPA Oil and Gas, 2006.
- [10] I. C. Evans, H. Solutions, C. Uk, M. J. Richards, and A. Corporation, "The Price of Poor Power Quality," in AADE National Technical Conference, 2011, pp. 0–12.
- [11] S. Acharya, X. She, M. H. Todorovic, R. Datta and G. Mandrusiak, "Thermal Performance Evaluation of a 1.7-kV, 450-A SiC-MOSFET Based Modular Three-Phase Power Block with Wide Fundamental Frequency Operations," in *IEEE Transactions on Industry Applications*, vol. 55, no. 2, pp. 1795-1806, March-April 2019
- [12] L. Zhang, X. Yuan, X. Wu, C. Shi, J. Zhang and Y. Zhang, "Performance Evaluation of High-Power SiC MOSFET Modules in Comparison to Si IGBT Modules," in *IEEE Transactions on Power Electronics*, vol. 34, no. 2, pp. 1181-1196, Feb. 2019.
- [13] S. Madhusoodhanan, K. Mainali, A. K. Tripathi, A. Kadavelugu, D. Patel and S. Bhattacharya, "Power Loss Analysis of Medium-Voltage Three-Phase Converters Using 15-kV/40-A SiC N-IGBT," in *IEEE Journal of Emerging and Selected Topics in Power Electronics*, vol. 4, no. 3, pp. 902-917, Sept. 2016.
- [14] T. Hennig, D. Mende and L. Hofmann, "Efficiency evaluation of offshore power systems with power electronics based on SiC technology," 2016 IEEE PES Asia-Pacific Power and Energy Engineering Conference (APPEEC), Xi'an, 2016, pp. 634-639.
- [15] B. Hu *et al.*, "A Survey on Recent Advances of Medium Voltage Silicon Carbide Power Devices," 2018 *IEEE Energy Conversion Congress and Exposition (ECCE)*, Portland, OR, 2018, pp. 2420-2427.
- [16] G. Wang *et al.*, "A Review of Power Electronics for Grid Connection of Utility-Scale Battery Energy Storage Systems," in *IEEE Transactions on Sustainable Energy*, vol. 7, no. 4, pp. 1778-1790, Oct. 2016.
- [17] ABB "Applying IGBTs" I Application Note 5SYA 2053-04
- [18] T. H. Duong, J. M. Ortiz-Rodriguez, R. N. Raju and A. R. Hefner, "Electro-thermal simulation of a 100 A, 10 kV half-bridge SiC MOSFET/JBS power module," 2008 IEEE Power Electronics Specialists Conference, Rhodes, 2008, pp. 1592-1597
- [19] A. Reznik, M. G. Simões, A. Al-Durra and S. M. Mueeen, "LCL Filter Design and Performance Analysis for Grid-Interconnected Systems," in *IEEE Transactions on Industry Applications*, vol. 50, no. 2, pp. 1225-1232, March-April 2014.
- [20] ABB, "IGBT Module datasheet- 5SNA 0400J650100".
- [21] F. P. Marafão, D. I. Brandão, A. Costabeber and H. K. M. Paredes, "Multi-task control strategy for grid-tied inverters based on conservative power theory," *IET Renewable Power Generation*, vol. 9, no. 2, pp. 154-165, 2015.
- [22] T. E. N. Zuniga and J. A. Pomilio, "Shunt active power filter synthesizing resistive load," *IEEE Transactions on Power Electronics*, vol. 16, no. 2, pp. 273-278, 2002.
- [23] D. Johannesson, M. Nawaz and K. Ilves, "Assessment of 10 kV, 100 A Silicon Carbide mosfet Power Modules," in *IEEE Transactions on Power Electronics*, vol. 33, no. 6, pp. 5215-5225, June 2018.